Superconductivity in the van der Waals crystal SnS$_2$ up to 105 GPa

Binbin Yue,[1,*] Wei Zhong,[1] Xiaohui Yu,[2,3,4] and Fang Hong [2,3,4,†]

[1]*Center for High Pressure Science and Technology Advanced Research, 10 East Xibeiwang Road, Haidian, Beijing 100094, China*
[2]*Beijing National Laboratory for Condensed Matter Physics, Institute of Physics, Chinese Academy of Sciences, Beijing 100190, China*
[3]*School of Physical Sciences, University of Chinese Academy of Sciences, Beijing 100190, China*
[4]*Songshan Lake Materials Laboratory, Dongguan, Guangdong 523808, China*

The manipulation of electronic properties in layered materials is of great importance for both device design and fundamental research. Here, we report the pressure engineering on SnS$_2$, a typical van der Waals crystal with promising application in the field of photonic and electronic devices, which is a semiconductor with a large band gap at ambient condition. The band gap was tuned by pressure from ∼2.2 eV at ambient condition to ∼0.6 eV at 30.7 GPa, and then SnS$_2$ became a metal near 35 GPa. Upon further compression, superconducting (SC) transition was observed above ∼50 GPa, and the SC critical temperature T_c increased with pressure, reaching ∼6.0 K at ∼105 GPa. Since there is much similarity with MoS$_2$ and/or other metal dichalcogenides, SnS$_2$ provides an extra platform to investigate the pressure-driven superconductivity in the large metal dichalcogenide family, which benefits the exploration of new superconductors and underlying mechanisms as well.

I. INTRODUCTION

Metal dichalcogenides MX_2 ($X =$ S, Se, Te) are a large material family with diverse physical properties, which attract attention in various fields. Most of these compounds are in the form of a layered structure and have similar hexagonal lattice symmetry with graphene, while they can also exist in other forms with different symmetries by controlling the synthesis conditions. Metal dichalcogenides provide an ideal platform to achieve rich physics and functions [1], such as charge density wave (CDW), superconductivity (SC), and Mott transition [2]. The weak interlayer interaction allows mechanical exfoliation, and few-layer or monolayer compounds can be obtained, which is of great benefit for application in flexible electronic and photonic devices [3]. Pressure engineering has been a powerful tool to tune the physical properties of MX_2 materials since the interlayer interaction is sensitive to external pressure. External pressure was found to enhance the superconducting transition in 2H-TaS$_2$ from initially below 1 K to 8.5 K at 9.5 GPa and suppresses the CDW [4]. A recent study shows that higher pressure can achieve a record-high SC transition in 2H-TaS$_2$ with a $T_c \approx 16.4$ K at 157.4 GPa [5]. Pressure-enhanced superconductivity was also observed in 2H-NbS$_2$ [6,7] and 2H-NbSe$_2$ [7–9], and the superconductivity in 2H-NbSe$_2$ was found to be not sensitive to the CDW [10]. The pressure can also induce metallization and superconductivity in some semiconducting or semimetallic MX_2 compounds, such as 2H-MoS$_2$ [11,12] and 1T-TaS$_2$ [13,14]. In 2M-WS$_2$, pressure induced a structural phase transition to a 3R phase at 15 GPa, while the compound transformed from a superconductor to a semiconductor, and the 3R phase became a metal and superconductor again under higher pressure [15].

As an important member in the large MX_2 material family, SnS$_2$ has been investigated due to its exotic physical and chemical properties, which draw considerable attention in the fields of optoelectronic detectors [16,17], photochemical catalysts [18,19], photovoltaics [20], and even field-effect transistors [21]. For realistic application, SnS$_2$ also has its own advantages, such as the cheap price, abundance, and being environmentally friendly. Similar with other layered metal dichalcogenides, SnS$_2$ is sensitive to external strain and pressure. Theoretical calculation shows that a 2.98% biaxial tensile strain can drive the indirect-direct band gap transition in bulk SnS$_2$ crystal, while a 9.75% biaxial tensile strain can transform the compound from the semiconducting state to a metallic state [22]. The structure is found to be stable under normal compressive strain up to −24%, at which SnS$_2$ becomes a metal [23]. The pressure effect on SnS$_2$ was studied by both the theoretical calculation and the experiments. The compressibility of this compound is highly anisotropic below 10 [24] or 20 GPa [25]. The compressibility of the c axis of SnS$_2$ is similar with those in graphene and hexagonal boron nitride, and much easier to be compressed than that in MoS$_2$ [25,26]. The shortening of S-S interlayer bonding in SnS$_2$ is strongly correlated to the electronic structure [25]. Density functional theory calculations predicted a semiconductor-metal transition in SnS$_2$ near 33 GPa [25], and SnS$_2$ could be a superconductor similar to SnSe$_2$ under nonhydrostatic compression [27]. Though there are already several high-pressure studies on SnS$_2$, the transport property is still not reported. Here, we studied SnS$_2$ by combining electric transport, optical absorption, and Raman spectroscopy characterization. SnS$_2$ is confirmed to be a superconductor

---

*yuebb@hpstar.ac.cn
†hongfang@iphy.ac.cn

above 50.5 GPa and has an unexpected T_c of around 6.0 K at 105 GPa, and the T_c could be higher if higher pressure is applied. The optical measurement revealed the process of semiconductor-metal transition and an underlying phase transition, which may be a $2H_c$-$2H_a$ isostructural phase transition.

II. EXPERIMENTS

The temperature-dependent electric resistance under high pressure was measured via the standard four-probe geometry in a commercial cryostat from 1.7 to 300 K by a Keithley 6221 current source and a 2182 A nanovoltmeter. A BeCu alloy diamond-anvil cell (DAC) with two opposing anvils was used to generate high pressure. For pressure less than 50 GPa, 300 μm culets were used while 100 μm culets were used for higher pressure. In these experiments, the bulk crystal was firstly exfoliated to a thin flake with thickness less than 5 μm and then a small piece of sample was cut from the thin flake. This small piece of sample was loaded into the sample chamber in a rhenium gasket with a c-BN insulating layer. Four Pt electrodes were placed on the surface of the samples in the chamber. KBr was used as the pressure medium. A ruby ball was loaded to serve as the internal pressure standard for pressure lower than 60 GPa, above which the Raman signal of the diamond culet was used to calibrate the pressure.

The high-pressure Raman spectra were collected using a Renishaw micro-Raman spectroscopy system equipped with 633 and 532 nm solid state lasers. The laser spot size is 1–2 μm. A pair of low fluorescent diamonds was used for Raman measurement. The laser power was maintained at a relatively low power level to avoid overheating during measurements. Two sets of Raman experiments were performed by using KBr and silicone oil as pressure mediums, respectively. *In situ* high-pressure ultraviolet-to-visible-to-near-infrared (UV-VIS-NIR) absorption spectroscopy was performed on a home-designed spectroscopy system (Ideaoptics, Shanghai, China) by using KBr as the pressure medium.

III. RESULTS AND DISCUSSION

The pristine SnS_2 crystal shows a shallow yellow color and is highly transparent. The initial resistances of the samples were briefly checked by a multimeter (two-probe method) and were on the scale of MΩ. The high-pressure transport measurement results with two sets of runs (four-probe method) are presented in Fig. 1. In each run, the thickness and size of the samples were a little bit different, and this gave different initial resistances. Figure 1(a) is the result of the first run (Run 1) and the highest pressure was 41.6 GPa, while Figs. 1(b)–1(d) display the results of the second run (Run 2) in which the highest pressure was 105 GPa. At low pressure range ($P < \sim 35$ GPa), the R-T curves show typical semiconducting behavior, and the pressure enhanced the conductivity of SnS_2 monotonously. Near 35 GPa, as seen in Fig. 1(a), the R-T curve at high temperature range started to show metallic behavior while there was an upturn trend below ~ 120 K, suggesting the semimetal character. It has to be noted that the metallization transition near 35 GPa is in good agreement with the theoretical prediction, in which the metallization
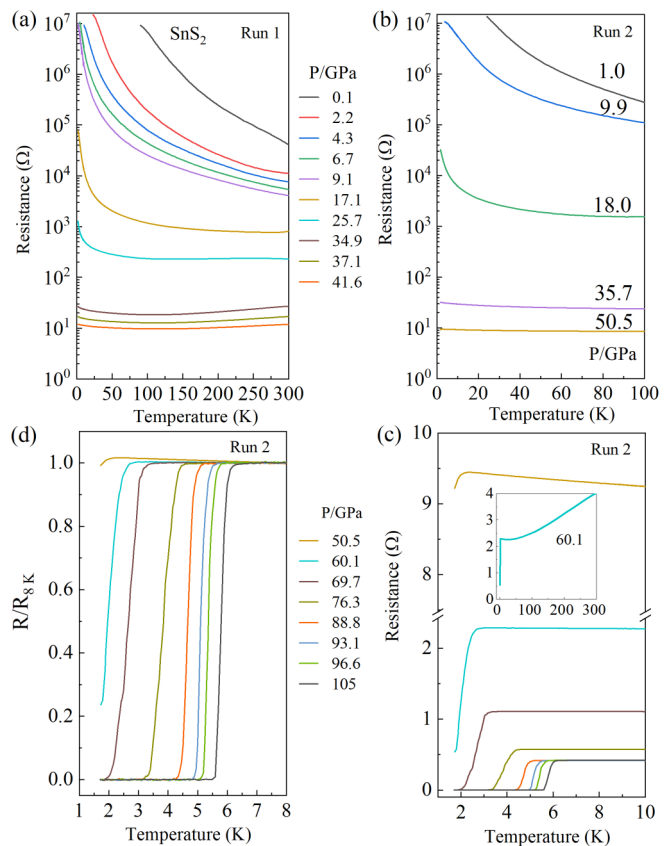
FIG. 1. The electric transport properties of SnS_2 under various pressures. (a) R-T results up to 41.6 GPa for Run 1. (b) R-T curves up to 50.5 GPa for Run 2, (c) R-T curves up to 105 GPa for Run 2; inset: the full temperature range data at 60.1 GPa. (d) Temperature-dependent normalized resistance at 8 K for Run 2. Note: (c) and (d) share the same color format and pressure legend.

pressure was estimated to be 33 GPa [25]. The upturn trend was further suppressed by higher pressure and the resistance dropped sharply below 2 K at 50.5 GPa, which could be a signal of possible superconducting transition, as seen in Fig. 1(c). To verify this superconducting transition in SnS_2, higher pressure was applied and a much sharper drop was observed at 60.1 GPa, while the sample became a metal clearly at high temperature range, as seen in the inset of Fig. 1(c). The zero-resistance state was achieved at ~ 1.8 K and 69.7 GPa. It is encouraging that the SC transition temperatures were elevated with pressure and reached ~ 6.0 K at 105 GPa, as seen in Fig. 1(c). To demonstrate the trend of superconducting transition clearly, Fig. 1(d) displays the normalized resistance at 8 K, and the same color format is adopted as that in Fig. 1(c). We also noted that the superconducting transition region became narrower with pressure. The superconducting transition is relatively sharp in SnS_2 and a zero-resistance state can be achieved, similar to the SC behavior in $2H$-TaS_2 [28], and different from the broad superconducting transition observed in MoS_2 without zero-resistance state [11]. Though SnS_2 has a larger band gap than MoS_2 at ambient condition, the superconducting transition pressure is much lower, only half of that in MoS_2 [11]. As mentioned above, previous study demonstrated that the interlayer distance is much easier to be
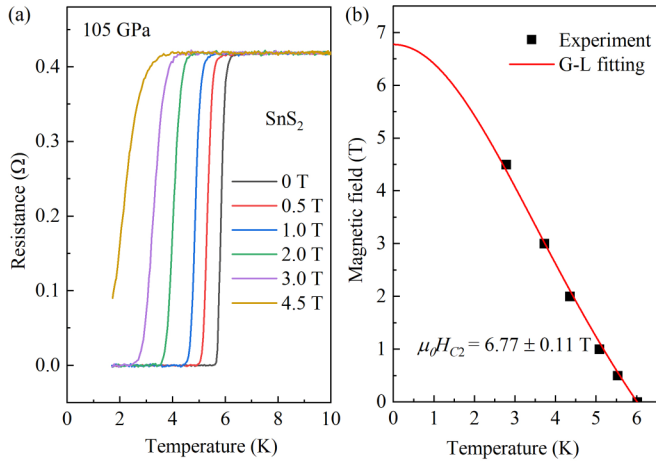
FIG. 2. The magnetic field effect on the superconducting transition of SnS$_2$ at ∼105 GPa. (a) R-T curves measured at various magnetic fields. (b) H-T_c relationship and G-L fitting.

FIG. 3. The absorption spectroscopy results of SnS$_2$ under high pressure. (a) Optical photographs of the sample inside DAC at selected pressures; (b) the optical absorption spectra collected at different pressures; (c) the optical band gap extracted from the absorption by fitting the curve with the Tauc relation.

compressed in SnS$_2$ than MoS$_2$ [25,26], and this may play an important role in the low critical pressure of the SC transition. The SC transition temperature of SnS$_2$ is almost identical to its sister SnSe$_2$ [29], although the SC critical pressure is different. It is noted that the T_c is robust in SnSe$_2$ above 30 GPa while the T_c is still not saturated in SnS$_2$ at 105 GPa. Considering the recently reported 16.4 K T_c in TaS$_2$ at 157.4 GPa [5], it is possible to get a higher T_c in SnS$_2$ by applying higher pressure. It is worthy to note that there is no signature of CDW observed in SnS$_2$ in the whole temperature and pressure ranges, which is different from the typical CDW compounds, such as TaS$_2$/TaSe$_2$ [7,13,30], NbSe$_2$ [9,10], and NbS$_2$ [31].

To further confirm the superconductivity, the magnetic effect was investigated at 105 GPa. Figure 2(a) displays the superconducting transition region at various magnetic fields. The magnetic field was normal to the electric current direction and parallel to the ab plane. It is clear that the magnetic field suppressed the superconductivity and the transition temperatures shifted to lower temperature when increasing the field, while the transition region became wider. The T_c-H relation was extracted and presented in Fig. 2(b). By fitting the T_c-H relation with G-L function, we obtained the zero-temperature upper magnetic field of SnS$_2$ at 105 GPa, $\mu_0 H_{C2} = 6.77 \pm 0.11$ T, which is lower than the BCS weak-coupling Pauli paramagnetic limit of $\mu_0 H_p = 1.84 T_c = 11.04$ T for $T_c = 6.0$ K, suggesting a phonon-mediated superconductivity. The phonon-mediated superconductivity was also supported by the theoretical calculation [27]. Apart from MoS$_2$ [11] and SnSe$_2$ [29], SnS$_2$ provides an extra opportunity and a reference sample without CDW to study the superconducting mechanism in the MX_2 material family. In the case of 1T-TaS$_2$, there are both competition and weak correlation between superconductivity and CDW, depending on the pressure range: at pressure less than 1 GPa, the SC and commensurate CDW compete with each other, while the SC coexists with the nearly commensurate CDW phase but is not sensitive to this phase [13]. There was a coexisting region between SC and CDW in the case of 2H-TaS$_2$, and the T_c continued to increase after full suppression of CDW,
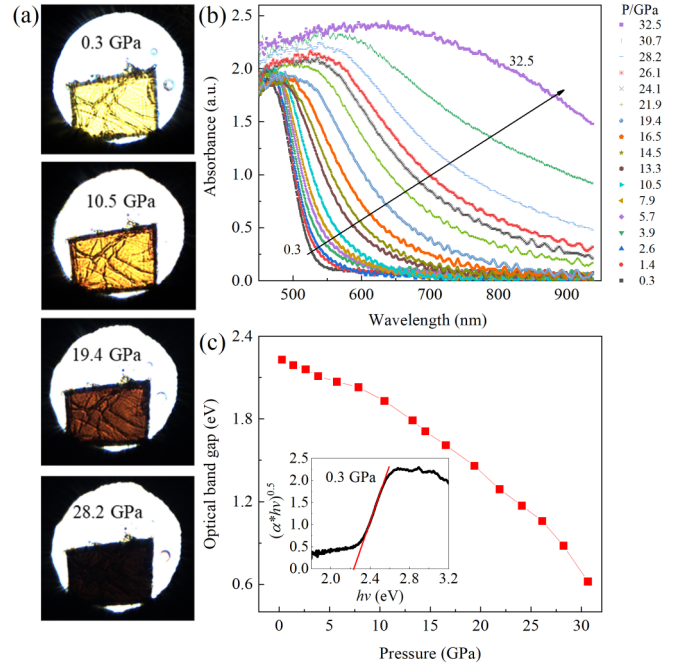
suggesting not a simple competition behavior between these two orderings [28]. The behavior is different in 2H-NbSe$_2$, which shares a similar structure with 2H-TaS$_2$; the CDW is found to boost superconductivity at an early stage [32]. However, the phonon study revealed that the superconductivity is actually not sensitive to the CDW in 2H-NbSe$_2$ [10]. It seems that the relationship between the CDW and SC is still a mystery in these metal dichalcogenides; at least it is highly dependent on the materials themselves and analysis methods, and it is hard to come to a universal and consistent conclusion. In the case of 2H-MoS$_2$ without CDW, the superconductivity may be linked to the emergence of a new flat hole-type Fermi pocket [11]. The superconductivity observed in SnSe$_2$ was similar to a p-wave-like unconventional superconductivity [29]. Hence, the superconductivity observed in these metal dichalcogenides looks much more complicated when more MX_2 superconductors are reported. Further theoretical work and advanced experimental characterization under high pressure are still required to reveal the underlying mechanism of MX_2 superconductivity.

The electronic structure evolution of SnS$_2$ under high pressure before metallization was investigated by the optical UV-VIS-NIR absorption measurement up to 32.5 GPa, as seen in Fig. 3. The left panel presents the images of samples inside the DAC at selected pressures, as seen in Fig. 3(a). The original sample was transparent with a shallow yellow color. At 10.5 GPa, it already changed to orange and then turned into brown at 19.4 GPa. The color of the SnS$_2$ crystal became almost black when the pressure was 28.2 GPa. The UV-VIS-NIR absorption spectroscopy provides much more delicate information and the absorption spectrum at 0.3 GPa
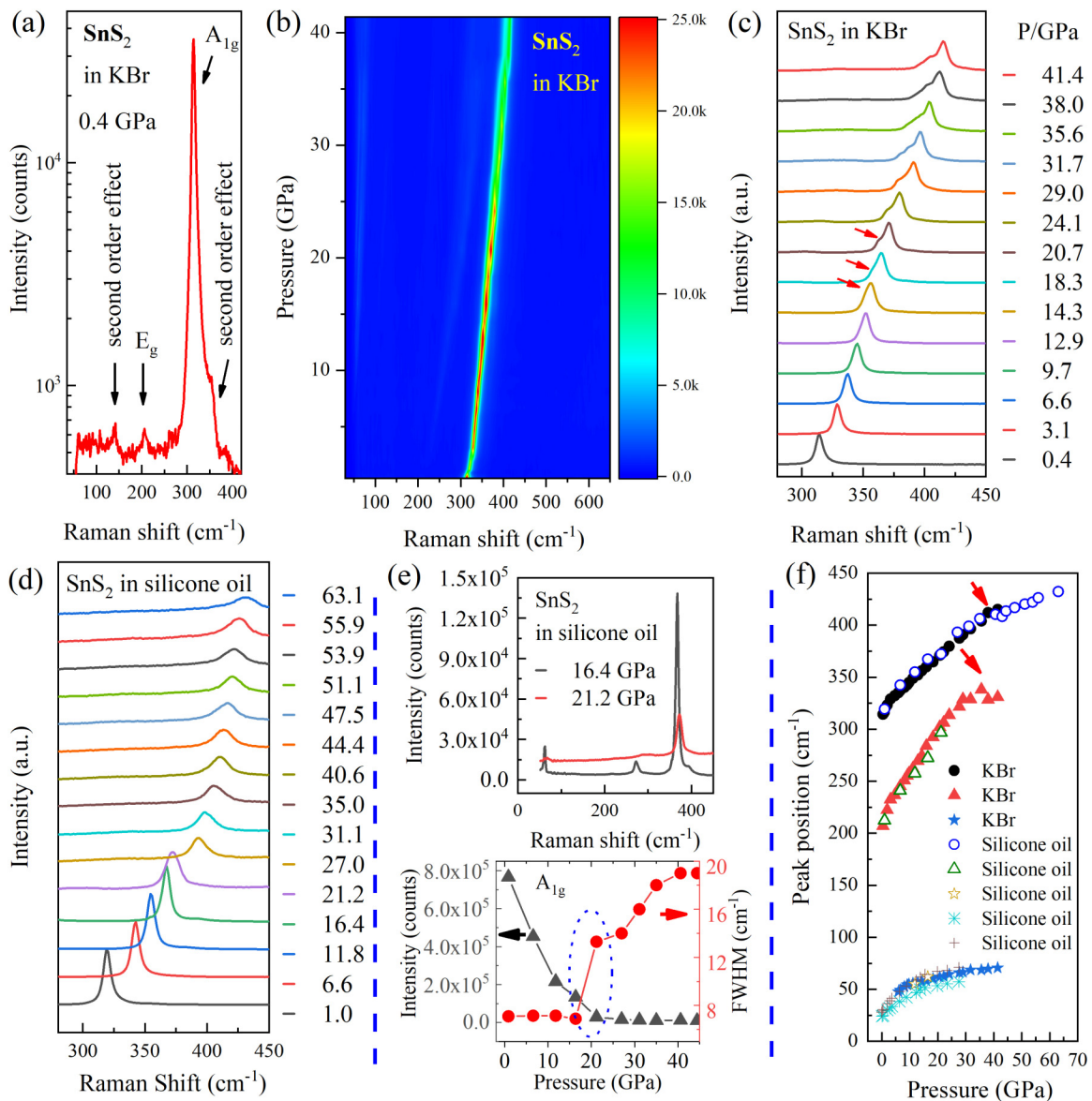
FIG. 4. Raman spectra of SnS_2 under high pressure. (a)–(c) Raman spectra collected from SnS_2 by using KBr as the pressure medium. (a) The spectrum of SnS_2 at 0.4 GPa. To reduce the contrast between weak and strong peaks, the intensity of the Raman signal was given in form of a logarithm format. (b) The two-dimensional contour plot of Raman spectra. (c) Line plot of selected Raman spectra, showing the enlarged region from 280 to 450 cm^{-1}. (d),(e) Raman spectra collected from SnS_2 by using silicone oil as the pressure medium. (f) The pressure-dependent Raman shifts in KBr and silicone oil.

shows a sharp optical absorption edge near 550 nm, which corresponds to an indirect optical band gap of ~2.25 eV and is well consistent with previous results [33–35]. Upon further compression, the absorption edges shifted to longer wavelengths and became wider, as indicated by the arrow in Fig. 3(b). The shift of absorption edge suggests the reduction of the optical band gap. By fitting the absorption spectra with the Tauc equation $(\alpha h\nu)^{0.5} = A(h\nu - E_g)$, the optical band gaps were obtained and presented in Fig. 3(c). Since the absorption data collected at 32.5 GPa is too broad and it is not sufficient for an acceptable Tauc plot fitting, Fig. 3(c) only shows optical band gap evolution up to 30.7 GPa. The broadening behavior at 32.5 GPa is to some extent consistent with

the metallization behavior observed near 35 GPa by transport measurement.

The structure evolution of SnS_2 under high pressure was checked by Raman spectroscopy up to 41.4 GPa by using KBr as the pressure medium, as displayed in Figs. 4(a)–4(c). At 0.4 GPa, a strong vibration mode was observed at ~314.5 cm^{-1} (A_{1g} mode), while there are two weak modes at ~206.3 (E_g mode) and 140.3 cm^{-1} (second-order effect), as seen in Fig. 4(a). The shoulder of the A_{1g} mode is also induced by the second-order effect [36]. This is well consistent with a previous Raman study [36], suggesting the high quality of the single-crystal sample. Upon compression, the A_{1g} and E_g vibration modes shifted to higher energy, suggesting a stronger

interaction between nearby atoms, while the 140.3 cm^{-1} mode was too weak to be visible under high pressure, as seen in Fig. 4(b). Both of them became wider and wider, which may be due to the quasihydrostatic pressure environment by using the solid KBr as the pressure medium. Meanwhile, the local slip and/or distortion of layered SnS$_2$ may also cause the widening behavior of Raman vibration. An extra mode near 50 cm^{-1} started to show above $\sim$10 GPa, below which this mode was not detected due to the cutoff limit of the Raman instrument, and it should be the E_2^3 quasi-rigid-layer mode (it is 28.5 cm^{-1} at 295 K) [36]. This mode was confirmed by the low wave-number Raman experiment and the peak position was $\sim$ 27.7 cm^{-1}, as seen in Fig. S1 in the Supplemental Material [37]. To check the possible hidden phase transition, the region between 280 and 450 cm^{-1} (the main Raman mode) of selected pressures was zoomed-in in Fig. 4(c) by line plots. As indicated by the red arrows in Fig. 4(b), there was a shoulder coming out from 18.3 GPa which became much clearer at 20.7 GPa. The critical pressure for this shoulder could be traced back to 14.3 GPa, at which the main peak is a little bit broad and asymmetric, compared with those below 14.3 GPa. Previous x-ray diffraction on single-crystal SnS$_2$ showed that there is no phase transition observed up to 20 GPa (the upper limit of the experiment) [25]. In addition, high-pressure work on the sister compound SnSe$_2$ shows that SnSe$_2$ did not experience any structure phase transition up to 46 GPa [29]. Generally, metal disulfides are also much stabler than their sister selenide. Considering the structure similarity between SnS$_2$ and SnSe$_2$, SnS$_2$ should be stable up to the highest pressure 41.4 GPa in Raman experiment. However, we also noted that there were several works reporting the thermodynamic instability of the pristine phase in SnS$_2$ and SnSe$_2$ [27,38]. Both the theoretical calculation and the single-crystal experiment were performed on SnSe$_2$, in which a superlattice stemming from the commensurate periodic lattice distortion (PLD) was observed above 17 GPa [38]. The PLD phase was also predicted to exist in SnS$_2$ above 20 GPa under hydrostatic condition [27]. In this case, it is possible that SnS$_2$ underwent the PLD phase transition near 20 GPa, deduced by the splitting of the A_{1g} mode. Another possibility is that SnS$_2$ underwent the 2H-4H phase transition [36], since there were no extra Raman modes appearing beyond the splitting of the A_{1g} mode, and the anisotropic compression behavior and the enhanced interlayer interaction could split the main degenerate vibration modes in the 4H phase [36]. We also noted that an isosymmetric phase transition from the 2H_c to the 2H_a phase was confirmed to occur in MoS$_2$ near 23 GPa by high-pressure single-crystal x-ray diffraction [39]. Similar behavior was also observed in compressed WS$_2$, in which different phase transition routes were found in different pressure mediums [40]. To figure out the possible effect of hydrostatic condition, we carried out another Raman experiment on SnS$_2$ by using silicone oil as the pressure medium up to 63.1 GPa, and the results of the main vibration mode are presented in Fig. 4(d). Different from the results by using KBr as the pressure medium, there is no clear splitting of the main mode. In this case, the splitting behavior of the main mode in KBr stems from the nonhydrostatic environment. In the case of the silicone oil experiment, we observed both the broadening and sharp drop of intensity of the main mode starting from
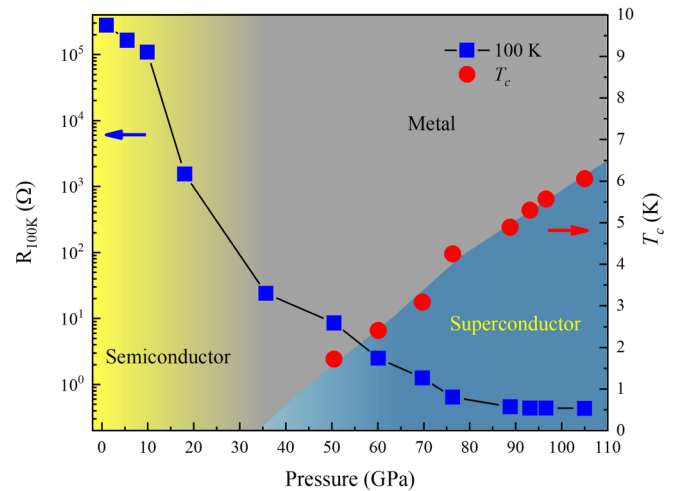
FIG. 5. The proposed *P-T* phase diagram of SnS$_2$.

21.2 GPa, as seen in Figs. 4(d) and 4(e). By comparing our results with those in 2H-WS$_2$ [40] and 2H-MoS$_2$ [39], similar 2H_c-2H_a phase transition may apply to SnS$_2$ near 20.7 GPa (in KBr) or 21.2 GPa (in silicone oil) rather than the PLD phase transition as mentioned above. A high-resolution x-ray diffraction experiment on SnS$_2$ is still required to reveal the accurate structural information and possible phase transition route under high pressure. Figure 4(f) presents the pressure-dependent Raman peak positions of SnS$_2$ collected in KBr and silicone oil, respectively. It is noted that there is some anomaly near 35 GPa, which is consistent with the metallization behavior.

Based on the transport measurement, a *P-T* phase diagram is proposed, as seen in Fig. 5. The resistance at 100 K of the SnS$_2$ sample decreased monotonously with pressure (data is collected from Run 2). Below 10 GPa, the resistance is on a scale of 10^5 Ω, the pressure-dependent change is relatively small, and this behavior is also consistent with the band gap changing as presented in Fig. 3(c), in which the band gap declined relatively slowly below $\sim$10 GPa. There is a big drop near 20 GPa, which corresponds to a possible 2H_c-2H_a phase transition. Near 35 GPa, SnS$_2$ started to transform from the semiconductor to a metal; the resistance at 100 K was only $\sim$24 Ω, reduced by at least four orders of magnitude. The metallic behavior became stronger and stronger while the superconducting transition started to emerge near 2 K at 50.5 GPa. Further compression enhanced the T_c and the highest T_c in this work was $\sim$6.0 K at 105 GPa, which may be further enhanced by applying higher pressure. By extrapolating the T_c -*P* relation to zero temperature, the initial SC transition may start as early as $\sim$35 GPa, where metallization just appeared.

IV. CONCLUSION

van de Waals layered crystal SnS$_2$ was investigated by electric transport, optical absorption, and Raman spectroscopy under high pressure. SnS$_2$ was found to be a superconductor above 50.5 GPa; T_c increased with pressure and reached $\sim$6.0 K at 105 GPa. The absorption results reveal the monotonous decreasing trend of the optical band gap below $\sim$35 GPa, above which SnS$_2$ started to transform from the

semiconductor to a metal. This work has demonstrated the pressure-induced superconductivity in SnS_2 with a relatively large initial band gap, which not only extends our knowledge on this promising compound but also is beneficial for the superconducting mechanism study in the large MX_2 material family.

[1] S. Manzeli, D. Ovchinnikov, D. Pasquier, O. V. Yazyev, and A. Kis, Nat. Rev. Mater. **2**, 17033 (2017).

[2] A. H. Castro Neto, Phys. Rev. Lett. **86**, 4382 (2001).

[3] L. Zheng, X. Wang, H. Jiang, M. Xu, W. Huang, and Z. Liu, Nano Res. **15**, 2413 (2022).

[4] D. C. Freitas, P. Rodière, M. R. Osorio, E. Navarro-Moratalla, N. M. Nemes, V. G. Tissen, L. Cario, E. Coronado, M. García-Hernández, S. Vieira, M. Núñez-Regueiro, and H. Suderow, Phys. Rev. B **93**, 184512 (2016).

[5] Q. Dong, J. Pan, S. Li, Y. Fang, T. Lin, S. Liu, B. Liu, Q. Li, F. Huang, and B. Liu, Adv. Mater. **34**, 2103168 (2022).

[6] V. G. Tissen, M. R. Osorio, J. P. Brison, N. M. Nemes, M. García-Hernández, L. Cario, P. Rodière, S. Vieira, and H. Suderow, Phys. Rev. B **87**, 134502 (2013).

[7] A. Majumdar, D. VanGennep, J. Brisbois, D. Chareev, A. V. Sadakov, A. S. Usoltsev, M. Mito, A. V. Silhanek, T. Sarkar, A. Hassan, O. Karis, R. Ahuja, and M. Abdel-Hafiez, Phys. Rev. Mater. **4**, 084005 (2020).

[8] D. Jérome, A. J. Grant, and A. D. Yoffe, Solid State Commun. **9**, 2183 (1971).

[9] C. Berthier, P. Molinié, and D. Jérome, Solid State Commun. **18**, 1393 (1976).

[10] M. Leroux, I. Errea, M. Le Tacon, S.-M. Souliou, G. Garbarino, L. Cario, A. Bosak, F. Mauri, M. Calandra, and P. Rodière, Phys. Rev. B **92**, 140303(R) (2015).

[11] Z. Chi, X. Chen, F. Yen, F. Peng, Y. Zhou, J. Zhu, Y. Zhang, X. Liu, C. Lin, S. Chu, Y. Li, J. Zhao, T. Kagayama, Y. Ma, and Z. Yang, Phys. Rev. Lett. **120**, 037002 (2018).

[12] Z.-H. Chi, X.-M. Zhao, H. Zhang, A. F. Goncharov, S. S. Lobanov, T. Kagayama, M. Sakata, and X.-J. Chen, Phys. Rev. Lett. **113**, 036802 (2014).

[13] B. Sipos, A. F. Kusmartseva, A. Akrap, H. Berger, L. Forró, and E. Tutiš, Nat. Mater. **7**, 960 (2008).

[14] B. Wang, Y. Liu, X. Luo, K. Ishigaki, K. Matsubayashi, W. Lu, Y. Sun, J. Cheng, and Y. Uwatoko, Phys. Rev. B **97**, 220504(R) (2018).

[15] W. Zhang, Y. Fang, Z. Zhang, F. Tian, Y. Huang, X. Wang, X. Huang, F. Huang, and T. Cui, J Phys. Chem. Lett. **12**, 3321 (2021).

[16] L. Gao, C. Chen, K. Zeng, C. Ge, D. Yang, H. Song, and J. Tang, Light: Sci. Appl. **5**, e16126 (2016).

[17] G. Su, V. G. Hadjiev, P. E. Loya, J. Zhang, S. Lei, S. Maharjan, P. Dong, P. M. Ajayan, J. Lou, and H. Peng, Nano Lett. **15**, 506 (2015).

[18] G. Liu, Y. Qiu, Z. Wang, J. Zhang, X. Chen, M. Dai, D. Jia, Y. Zhou, Z. Li, and P. Hu, ACS Appl. Mater. Interfaces **9**, 37750 (2017).

[19] L. A. Burton, T. J. Whittles, D. Hesp, W. M. Linhart, J. M. Skelton, B. Hou, R. F. Webster, G. O'Dowd, C. Reece, and D. Cherns, J. Mater. Chem. A **4**, 1312 (2016).

[20] W. Chu, X. Li, S. Li, J. Hou, Q. Jiang, and J. Yang, ACS Appl. Energy Mater. **2**, 382 (2018).

[21] H. Song, S. Li, L. Gao, Y. Xu, K. Ueno, J. Tang, Y. Cheng, and K. Tsukagoshi, Nanoscale **5**, 9666 (2013).

[22] B. Ram and A. K. Singh, Phys. Rev. B **95**, 075134 (2017).

[23] B. Ram, A. Manjanath, and A. K. Singh, 2D Mater. **3**, 015009 (2016).

[24] K. Knorr, L. Ehm, M. Hytha, B. Winkler, and W. Depmeier, Physica Status Solidi B **223**, 435 (2001).

[25] M. Filsø, E. Eikeland, J. Zhang, S. Madsen, and B. Iversen, Dalton Trans. **45**, 3798 (2016).

[26] R. M. Hazen and L. W. Finger, Am. Mineral. **63**, 289 (1978).

[27] G. P. Kafle, C. Heil, H. Paudyal, and E. R. Margine, J. Mater. Chem. C **8**, 16404 (2020).

[28] X.-M. Zhao, K. Zhang, Z.-Y. Cao, Z.-W. Zhao, V. V. Struzhkin, A. F. Goncharov, H.-K. Wang, A. G. Gavriliuk, H.-K. Mao, and X.-J. Chen, Phys. Rev. B **101**, 134506 (2020).

[29] Y. Zhou, B. Zhang, X. Chen, C. Gu, C. An, Y. Zhou, K. Cai, Y. Yuan, C. Chen, H. Wu, R. Zhang, C. Park, Y. Xiong, X. Zhang, K. Wang, and Z. Yang, Adv. Electron. Mater. **4**, 1800155 (2018).

[30] B. Wang, Y. Liu, K. Ishigaki, K. Matsubayashi, J. Cheng, W. Lu, Y. Sun, and Y. Uwatoko, Phys. Rev. B **95**, 220501(R) (2017).

[31] M. Leroux, L. Cario, A. Bosak, and P. Rodière, Phys. Rev. B **97**, 195140 (2018).

[32] T. Kiss, T. Yokoya, A. Chainani, S. Shin, T. Hanaguri, M. Nohara, and H. Takagi, Nat. Phys. **3**, 720 (2007).

[33] A. Li, Q. Chen, P. Wang, Y. Gan, T. Qi, P. Wang, F. Tang, J. Z. Wu, R. Chen, L. Zhang, and Y. Gong, Adv. Mater. **31**, 1805656 (2019).

[34] S. Acharya and O. N. Srivastava, Physica Status Solidi A **65**, 717 (1981).

[35] X. Zhou, Q. Zhang, L. Gan, H. Li, and T. Zhai, Adv. Funct. Mater. **26**, 4405 (2016).

[36] A. Smith, P. Meek, and W. Liang, J. Phys. C: Solid State Phys. **10**, 1321 (1977).

[37] See Supplemental Material at http://link.aps.org/supplemental/10.1103/PhysRevB.105.104514 for low wavenumber Raman results at high pressure.

[38] J. Ying, H. Paudyal, C. Heil, X.-J. Chen, V. V. Struzhkin, and E. R. Margine, Phys. Rev. Lett. **121**, 027003 (2018).

[39] A. F. Goncharov, M. Bykov, E. Bykova, K. Glazyrin, V. Prakapenka, Z.-Y. Cao, and X.-J. Chen, Phys. Rev. B **102**, 064105 (2020).

[40] S. Duwal and C.-S. Yoo, J. Phys. Chem. C **120**, 5101 (2016).